A Nature Portfolio journal



https://doi.org/10.1038/s42003-025-08216-3

Anterior-posterior systematic deficits of cortical thickness in early-onset schizophrenia

Check for updates

Yun-Shuang Fan^{1,2}, Yong Xu ® ³, Bin Wan ® ², Wei Sheng⁴, Chong Wang⁴, Mi Yang¹, Sofie Louise Valk ® ^{2,5,6,7} ⋈ & Huafu Chen ® ^{1,4,7} ⋈

Schizophrenia is a neurodevelopmental condition with alterations in both sensory and association cortical areas. These alterations have been reported to follow structural connectivity patterning, and to occur in a system-level fashion. Here we investigated whether pathological alterations of schizophrenia originate from an early disruption of cortical organization. We found a structural covariance gradient axis of cortical thickness discriminated anterior from posterior region and was compressed in early-onset schizophrenia (EOS) patients. Patients showed increased structural covariance between two ends of the anterior-posterior axis, with increased geodesic distance of covarying regions between two ends. Positive symptoms increased with the strengthening of structural covariance between two ends. Our findings revealed a contracted organizational axis in EOS patients, which was attributed to excessive distally coordinated changes between anterior and posterior cortical regions. Our study from a systematic perspective suggests disturbed maturational processes of cortical thickness in EOS, supporting the neurodevelopmental hypothesis of schizophrenia.

Schizophrenia is a psychiatric disorder associated with pathological changes in gray and white matter throughout the cerebral cortex¹. Although the behavioral manifestations of the disease usually appear in early adulthood, numerous neuroimaging studies suggest that the pathological process of the disease begins early in brain development². Early-onset schizophrenia (EOS), which is thought to be neurobiologically continuous with its adult counterpart³, provides an opportunity to study disease-specific aberrations in neurodevelopmental processes. Converging evidence suggests widespread alterations in cortical thickness in EOS patients, particularly in the frontal, temporal, and parietal regions^{4,5}. These gray matter changes have been suggested to follow the white matter organization of the cortex, consistent with models of disease propagation^{6–8}. However, it remains unclear how the maturational processes of cortical thickness are coordinately disturbed by the disease.

An intuitive method for capturing coordinated changes in cortical thickness across the cortex is the "structural covariance" approach. By calculating the covariance of cross-sectional cortical thickness data, this

approach measures the similarity of anatomical variations in the brain. The covariance pattern reflects the coordinated effects of specific micro- and mesoscopic factors, such as gene expression¹⁰, synaptogenesis¹¹, and laminar thickness¹². Moreover, the structural covarying pattern of childhoodadolescence reflects synchronized developmental changes in the cortex^{9,13} and serves as a signature of coordinated developmental processes¹³. For example, this structural covariance pattern has been shown to resemble intra-individual maturational coupling inferred from longitudinal data¹⁴. More optimal topological organization of structural covariance network is associated with higher cognitive performance, implying its involvement in the development of intelligence¹⁵. Altered covariance networks are related to a variety of mental health conditions in young patients with disorders such as depression¹⁶ and anxiety symptoms¹⁷. Patients with schizophrenia have an aberrant pattern of fronto-temporal, fronto-parietal, and fronto-thalamic covariations¹⁸, and show a disruption of covariance network architecture¹⁹. Atypical maturations of structural covariance have been shown in pediatric individuals at high risk for psychosis²⁰. Yet, few EOS studies investigated

¹The Clinical Hospital of Chengdu Brain Science Institute, School of Life Science and Technology, University of Electronic Science and Technology of China, Chengdu, China. ²Otto Hahn Group Cognitive Neurogenetics, Max Planck Institute for Human Cognitive and Brain Sciences, Leipzig, Germany. ³Department of Clinical Psychology, The Eighth Affiliated Hospital, Sun Yat-Sen University, Shenzhen, China. ⁴MOE Key Lab for Neuroinformation, High-Field Magnetic Resonance Brain Imaging Key Laboratory of Sichuan Province, University of Electronic Science and Technology of China, Chengdu, China. ⁵Institute of Neuroscience and Medicine (INM-7: Brain and Behavior), Research Centre Jülich, Jülich, Germany. ⁶Institute of Systems Neuroscience, Heinrich Heine University Düsseldorf, Düsseldorf, Germany. ⁷These authors contributed equally: Sofie Louise Valk, Huafu Chen. ⊠e-mail: valk@cbs.mpg.de; chenhf@uestc.edu.cn

maturational processes of cortical thickness at a high resolution of structural covariance network²¹.

Recently, brain maturation processes have been reported to occur in a system-like manner²². Systematic patterns of brain organization have been described within a framework of "gradients"23, that capture an orderly spatial progression of cortical features²⁴. For example, neuronal density changes systematically along spatially organized gradients²⁵. To characterize the systematic gradient pattern of cortical organization, a nonlinear dimensionality reduction technique, also called "diffusion embedding" has been proposed^{26,27}. By embedding cortical regions into a continuous gradient map according to the similarity of their structural covariance profiles, previous work has revealed a non-random spatial organization of structural coordination across the cortex^{28,29}. In particular, the dominant structural gradient axis tends to distinguish posterior cortices from anterior cortices, reflecting the temporal sequence of neurogenesis²⁸. Generally, the posterior portion of the cortex has a greater number of neurons with a shorter cell cycle, while the anterior end has a smaller number with a longer cell cycle³⁰. Common disease effects across various psychiatric disorders have been found to follow a similar cortical thickness covariance gradient axis dissociating anterior and posterior regions³¹. Accordingly, the anteriorposterior gradient axis of structural covariance shaped by neurodevelopmental mechanisms appears to be also affected by psychiatric conditions. Despite the potential interplay of development and illness effects on the gradient axis, it remains unknown whether the gradient patterns change in patients with EOS, and how the system-level disruptions relate to cortical thickness abnormalities.

The systematic pattern of brain organization is supported by many factors. Among them, physical distance along the cortical surface is an important determinant of how regions are connected and thus how the brain is organized³². Indeed, a previous quantitative retrograde tracer analysis of macaque cortical networks suggests that physically close areas are more likely to be interconnected³³. In addition to physical distance, anatomical similarity between regions is also an important determinant 12,34. For example, cortical regions with similar laminar thickness patterns have been reported to have higher structural and functional connectivity¹². In fact, physically close regions tend to have similar microstructural profiles and high interregional connectivity^{35,36}. A structural covariance network reflecting the similarity of anatomical variations in the brain has shown a bias toward short-distance connections¹³. Physical distance along the cortical surface has been suggested to be associated with system-level transitions of both microscale cortical cytoarchitectural covariance¹² and macroscale cortical thickness covariance²⁸. Together, physical distance, anatomical similarity, and brain connectivity seem to be intrinsically linked and are essential to the formation of the systematic pattern of brain organization. Here we would test the relationship between geodesic distances, anatomical similarities, and gradient patterns, and whether EOS affected it by examining the geodesic distance between covarying regions in patients.

To investigate whether macrostructural covariance is systematically altered in EOS patients, we first computed structural covariance of crosssectional cortical thickness data from 95 patients with antipsychotic-naive first-episode EOS and 99 typically developing (TD) controls (recruited sample of 99 EOS and 100 TD, 7–17 years-old)¹³. We then decomposed the similarity matrix of covariance into a low-dimensional embedding using the diffusion embedding approach²⁶. To further unravel the potential biological mechanisms behind system-level changes of cortical thickness in patients, we examined diagnosis and symptom effects on structural covariance patterns ordered by the covariance gradient axis in TD controls. Finally, we estimated covariance distances by calculating geodesic distance between covarying regions³⁷. Taken together, we found a structural gradient consistently describe an anterior-posterior transition mirroring the temporal sequence of neurogenesis²⁸, and was distorted by EOS. Contracted covariance gradient axis in EOS could be contributed to excessive distally coordinated changes between anterior and posterior regions of the cortex, and was associated with positive symptoms in patients.

Results

Patients with EOS (mean \pm SD = 2.58 \pm 0.45 mm) showed reduced global cortical thickness relative to TD controls (mean \pm SD = 2.62 \pm 0.46 mm; t = 2.41, p = 0.02), consistent with previous findings³⁸. To reveal system-level structural abnormalities of EOS patients, we calculated structural covariance gradients of cortical thickness for the TD and EOS groups (Fig. 1). Specifically, we decomposed the 90% thresholded covariance matrix into 10 gradient components and aligned gradient maps of EOS with normative gradient maps of TD controls. Along the gradient axis, the position of a region was determined by the similarity of its structural covariance profile to others, thus indicating opposite poles of the axis with maximally divergent covariance patterns. The first gradient component (G1) explained 20% of the variance in the TD group and 26% of the variance in the EOS group to distinguish motor regions from other cortical areas. The second gradient (G2) axis (explained eigenvariance: EOS group = 18%; TD group = 15%) was significantly related to the main structural covariance gradient axis derived from the Human Connectome Project (HCP) adult data (r = 0.69, p_{spin} < 0.0001) that distinguishing posterior cortices from anterior cortices²⁸, whereas the G1 map showed no correlation with either the HCP G1 map $(r = 0.22, p_{spin} = 0.18)$ or the HCP G2 map $(r = 0.20, p_{spin} = 0.28)$ (Supplementary Fig. S1). Hence, here we mainly focused on the G2 axis and further

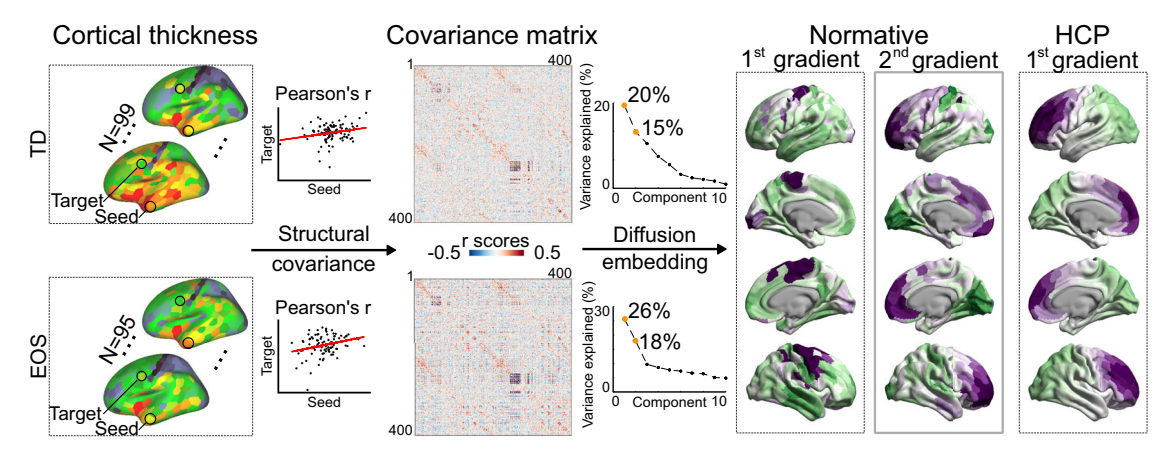


Fig. 1 | Method flowchart of the structural covariance gradient. Vertex-wise cortical thickness was first extracted and down-sampled to 400 parcels from the Schaefer atlas ⁵⁶. Structural covarying patterns were then estimated by using structural covariance of cortical thickness in typically developing (TD) controls, or early-onset schizophrenia (EOS) patients. After column-wise thresholding at 90%, the

covariance matrix was then decomposed into 10 low-dimensional components by using the diffusion embedding method. Only the second component in TD, i.e., the second normative gradient, was related with the gradient axis derived from the human connectome project (HCP) data²⁸, and thus selected-out and used in further analyses.

examined group differences between EOS and TD along this axis. See Supplementary Materials for further details about G1 maps.

Systematic covariance gradient maps

Similar to the well-established HCP gradient map²⁸, the G2 axis described a spatial arrangement from anterior to posterior regions in the cerebral cortex (Fig. 2A). Patients with EOS showed a compressed gradient axis compared to TD controls (Kolmogorov-Smirnov test; $D_{400} = 0.13$, p = 0.002). No parcels survived the false discovery rate (FDR) correction for z-score differences of gradient scores (Supplementary Fig. S2). After pooling 400 cortical parcels into seven functional networks, we observed that the posterior end was located in the visual network (VIS) and sensorimotor network (SMN), while the anterior end was anchored in transmodal networks, including the default mode network (DMN) and frontoparietal network (FPN) (Fig. 2B). No significant group difference in network-level gradient scores was found between the EOS and TD groups using paired t-tests. We then divided cortical parcels into 10 equal-sized bins according to their ranked gradient scores in TD controls and tested group differences for each bin by using paired t-tests (Fig. 2C). Patients showed increased gradient scores in the 3rd bin and decreased gradient scores in the 9th and 10th bins $(q_{FDR} < 0.05)$, indicating a disrupted segregation for both the posterior and anterior parts.

Group differences on structural covariance

To further investigate the compressed anterior-posterior axis in EOS patients, we reorganized and averaged the structural covariance matrices according to the 10-binned normative gradient mask (Fig. 3). Along the normative gradient axis, close ranks of two bins reflected similar structural covarying profiles. As expected, the further apart two bins were along the gradient axis, the lower the covariance value. We then tested for diagnosis effects on the reshaped structural covariance patterns. We found that patients had increased covariance values between the 1st and 9th bins $(t = 3.66, q_{FDR} = 0.002)$, i.e., less negative covariance values in EOS compared to TD (Fig. 3A). Here, the increased covariation between the anterior and posterior ends partly explained the abovementioned disruptions of gradient segregation. Additionally, we found more severe positive symptoms were related with reduced covariance between the 1st and 10th bins $(t = -3.01, q_{FDR} = 0.009)$ (Fig. 3B). More severe negative symptoms were related with increased covariance between the 10th and 6th bins (t = 2.71, $q_{FDR} = 0.02$).

Group differences on covariance distances

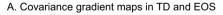
To examine the relationship between physical distances and structural covariance maps, we first computed node-wise geodesic distance degrees by averaging geodesic distances from one parcel to all other parcels (Fig. 4A), and found that it was relatively large in the frontal, inferior temporal, and occipital regions compared to other regions. The anterior-posterior gradient map was significantly related to the nodal degree map of geodesic distance $(r = 0.37, p_{spin} = 0.04)$. As expected, structural covariance was negatively correlated with geodesic distance (r = -0.20, $p_{perm} < 0.0001$), supporting previous findings of a short-distance connection bias in structural covariance networks13.

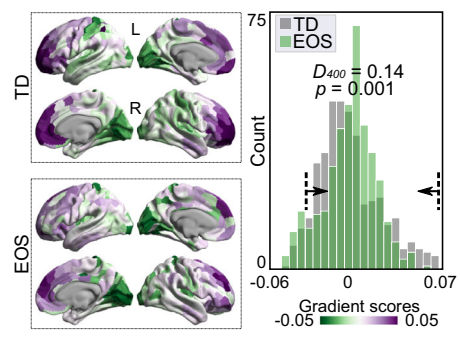
To further investigate the relationship between physical distances and covariance perturbations in EOS, we computed covariance distances by averaging the geodesic distance from a seed region to its covarying regions (Fig. 4B)³⁷. A high covariance distance score of a region indicates a pattern dominated by remote connectivity, and a low score indicates local connectivity. After resampling the covariance distance maps along the gradient axis (Fig. 4C), we found that patients showed increased covariance distances in both ends of the gradient axis, but decreased covariance distances in the middle of the axis. Specifically, patients with EOS showed statistically increased covariance distances in the 1st bin (t = 3.69, $q_{FDR} = 0.007$) and the 10th bin (t = 3.40, $q_{FDR} = 0.008$) compared to TD controls.

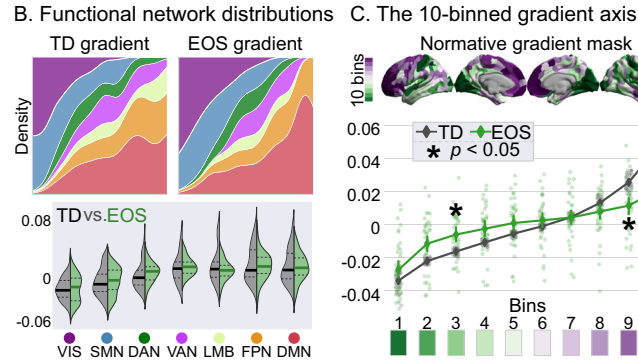
Discussion

In the current study, we investigated the system-level organization of coordinated structural changes in EOS patients by applying a dimensional reduction approach to the structural covariance of cross-sectional cortical thickness data. Similar to the principal gradient reflecting the temporal sequence of neurogenesis from the young adult HCP sample²⁸, G2 of the structural covariance pattern described an anterior-posterior organizational axis, capturing a unimodal-transmodal transition. Patients with EOS showed a contracted anterior-posterior gradient pattern compared to TD controls. In addition, patients showed increased structural covariance between the anterior and posterior ends of the gradient and increased covariance distances of both poles compared to TD controls. Taken together, these findings revealed a disrupted systematic organization of structural covariance patterns in EOS patients, which was supported by excessive distant connection profiles between the two ends of the axis.

Consistent with previous findings²⁸, our study revealed an anteriorposterior gradient axis of structural covariance in this young age group. However, it was the second, and not the first, covariance gradient of this age group that was aligned with the main covariance gradient in adults²⁸. The shift in macroscale cortical organization between pediatric and adult populations has been reported in functional connectivity gradients³⁹. This previous work concluded that these gradient order changes represent a maturation of cortical organization that may be critical for the refinement of cognitive and behavioral abilities during development. As previously







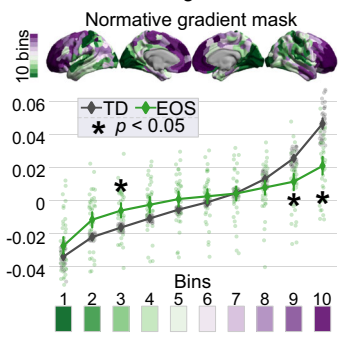


Fig. 2 | Structural covariance gradient patterns. A Covariance gradient maps in TD and EOS. In the right density map, green boxes represent gradient scores of EOS patients and gray boxes represent TD controls, which suggested compressed gradient axis in EOS than TD (Kolmogorov-Smirnov test; $D_{400} = 0.13$, p = 0.002). B Network distributions. For each group, the continuous density maps of gradient scores were separately plotted for each network. Group differences between EOS and

TD were tested by using paired *t*-tests [False discovery rate (FDR) corrections, q_{FDR} < 0.05]. VIS visual network, SMN sensorimotor network, DAN dorsal attention network, VAN ventral attention network, LMB limbic network, FPN frontoparietal network, DMN default mode network. C The 10-binned gradient axis. We computed bin-level gradient scores according to the 10-binned normative gradient mask and tested group differences by using paired t-tests (FDR corrected, p < 0.05).

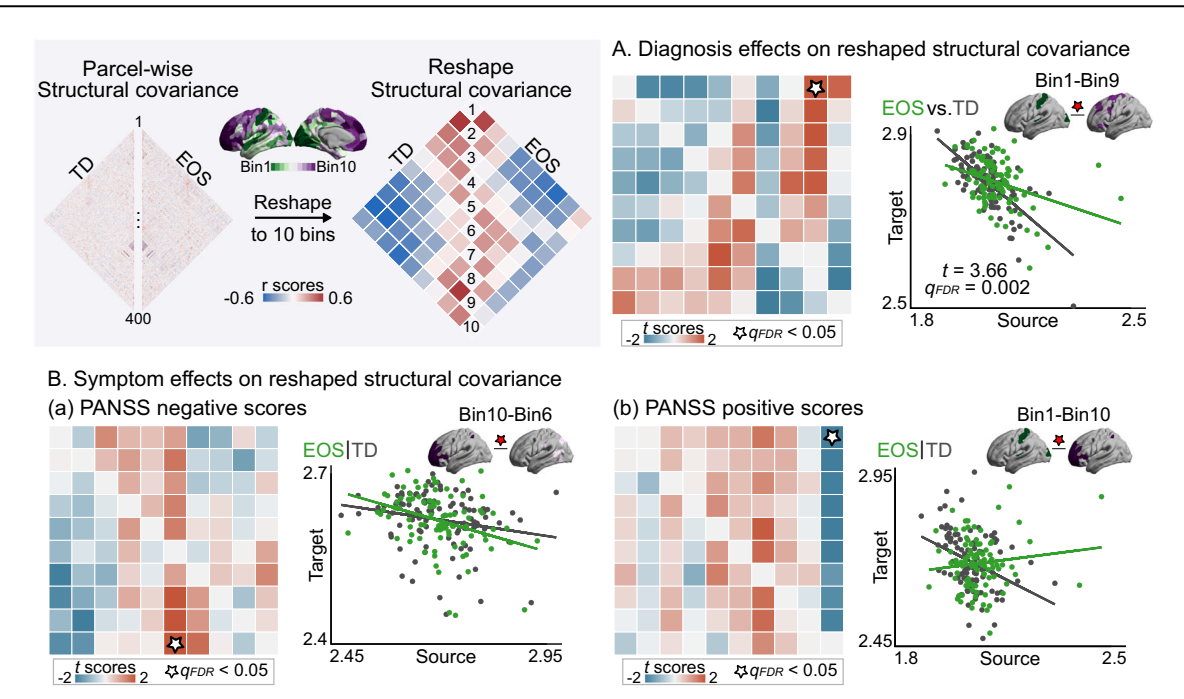


Fig. 3 | Disease effects on structural covariance patterns. Covariance matrices were reshaped into 10×10 matrices according to a 10-binned mask generated from the anterior-posterior gradient of TD controls. A Diagnosis effects on reshaped covariance. The diagnosis effect was examined by using a classic interaction linear model with group and cortical thickness as factors (FDR corrected, p < 0.05). Green dots and lines represent EOS patients and gray dots and lines represent TD controls.

B Symptom effects on reshaped covariance. We used N scores of the Positive and Negative Syndrome Scale (PANSS) to quantify the severity of negative symptoms, and PANSS-P scores for positive symptoms. In the EOS group, symptom effects were examined by the interaction linear model with PANSS-P/N scores and cortical thickness as factors (FDR corrected, p < 0.05).

suggested²⁸, the anterior-posterior axis appears to map the temporal sequence of neurogenesis. Specifically, the posterior and anterior portions of the cortex are distinguished by their neuronal counts, i.e., a greater number of neurons with a shorter cell cycle at the posterior end, and a smaller number with a longer cell cycle at the anterior end³⁰. Furthermore, this gradient axis has been suggested to be related to the functional continuum from basic perception to abstract cognition²⁸. Our findings of functional network distributions showed a similar unimodal-transmodal transition, supporting previous gradient findings in adults. Future longitudinal studies are needed to elaborate on dynamic changes in the anterior-posterior macrostructural axis from childhood to adulthood.

A previous study found compression of the sensorimotor-totransmodal functional connectivity gradient in patients with chronic adult-onset schizophrenia⁴⁰, and suggested that this was a system-level substrate underlying sensory and cognitive deficits of patients⁴¹. Consistently, we found compressed system-level covariance gradient axis in EOS patients, indicating that both structural and functional cortical organization were less dispersed in schizophrenia. The previous study suggested that reduced functional separation between primary sensory and fronto-parietal cognitive systems may contribute to the phenomenon of functional hierarchical compression. In the current study, we found similar reduced structural separation in EOS patients, i.e., increased structural covariance between posterior and anterior regions. During brain development, primary sensory cortices are relatively uncoupled from the rest of the cortex⁹, whereas frontotemporal cortices have stronger and more extensive coupling patterns, responsible for the involvement of integrative cognitive processes⁴². Therefore, patients' excessive structural coupling between posterior and anterior regions may provide a mechanistic explanation for compressed structural organization in EOS. We found that the clinical severity of positive symptoms decreased with the strengthening of structural coupling between posterior and anterior regions, suggesting a compensatory neural mechanism in EOS. Particularly, patient's increased structural coupling was a downstream alteration of the brain during the pathological process of schizophrenia, to achieve similar activity patterns in biological networks as the generation population⁴³. However, group differences of gradient scores could not be observed at the parcel level. We inferred that the parcel-wise overlap of cortical thickness between patients and controls (Supplementary Fig. S3A) might be responsible for this negative finding. Despite the parcel-wise overlap, patients with EOS exhibited systematic disruptions of cortical thickness, underscoring the critical need for future investigation from a system-level perspective.

Geodesic distance was correlated with the anterior-posterior covariance gradient, supporting the hypothesis that physical distance is an important determinant of cortical organization. Indeed, we found that regions with greater geodesic distance had lower structural covariance. However, we again found some distance-related differences between individuals with EOS and TD. By calculating the covariance distance, we tested the relationship between physical distance and systematic structural organizational changes in EOS. In general, sensory areas had more clustered local connections, whereas transmodal systems had distributed remote connections^{44–46}. The increased connectivity distance in association areas relative to sensory areas could be driven by multiple factors, reflecting a systematic balance between short- and long-distance connections. The "tethering hypothesis" relates this distribution of connectivity distance to evolutionary expansion⁴⁷. Specifically, this hypothesis views sensory regions as anchors and transmodal association cortex as the evolutionally expanding cortical areas tethering these anchors, potentially explaining the increase in long-range connectivity in association regions. We found that patients with EOS showed increased covariance distances of both sensory and transmodal systems, which is consistent with previous findings of distance-dependent miswiring patterns⁴⁸. According to a concept of network attributes⁴⁹, local connections are associated with functional system segregation, and longrange connections with integration. Therefore, increased covariance distances of sensory and transmodal systems in EOS patients might reflect disturbed network topology, potentially interpreting their contracted macroscale structural organization.

This study has several limitations about the elements of methodology and study design. First, given the young age of participants (7-17 years old),

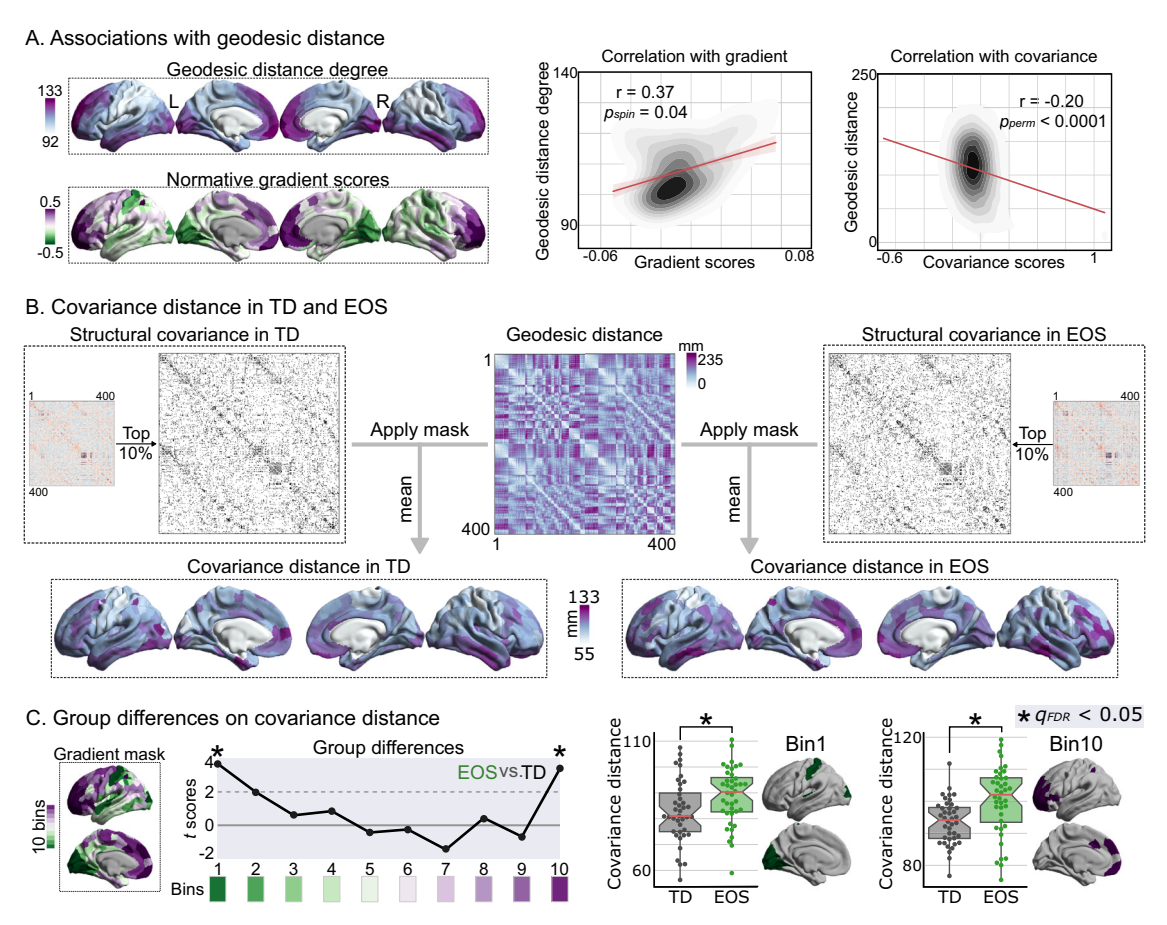


Fig. 4 | **Covariance distance in TD and EOS. A** Correlations between geodesic distances and covariance gradients and covariance matrices. The node-wise geodesic distance degree was calculated by averaging the geodesic distance for each node. The spin test was used to control for spatial autocorrelations (p_{spin} < 0.05, 10,000 times)⁶⁵. The edge-wise geodesic distance was then correlated with the structural covariance matrix, and the statistical significance was assessed using permutation tests (p_{perm} < 0.05, 10,000 times). **B** Covariance distance calculation. For each group, we column-wise thresholded the structural covariance matrix at 90%, and then

binarized it as a mask. Covariance distance was then calculated using the averaging geodesic distance profiles of a seed region multiplied by the mask. C Effects of disease on covariance distances. In the left line graph, one dot represents a bin along the normative gradient axis, showing t values evaluated by paired t-tests (* represents $q_{FDR} < 0.05$). In the right box-and-whisker plots, the red horizontal lines in the box indicate the mean of each group, and the lower and upper horizontal lines indicate the lower and upper quartiles, respectively. Green boxes represent covariance distances of EOS patients and gray boxes represent TD controls.

two senior psychiatrists with more than 10 years of experience made the consensus diagnosis by interviewing both the child and parent(s). However, it is still a major limitation that we did not use the Schedule for Affective Disorders and Schizophrenia Present and Lifetime Version for Children (K-SADS-PL) to assess symptoms and DSM-IV diagnoses of participants by semi-structured diagnostic interviewing the child and parent(s) separately. Thus, our findings of the anterior-posterior gradient axis in this young age group should be more carefully verified in the future. Second, the current study design was based on a cross-sectional dataset, which does not reflect co-maturation processes between different cortical regions in young individuals. Although population-based structural covariance of cortical thickness could be explained by subject-based maturational coupling patterns derived from longitudinal data¹⁴, further longitudinal studies are needed to validate the system-level perturbations of structurally coordinated changes in EOS patients. Third, in addition to the cerebral cortex, subcortical nuclei are also important pathological components in schizophrenia⁵⁰. We additionally computed a covariance gradient by combining cortical areas and subcortical regions, including the accumbens, amygdala, caudate, hippocampus, pallidum, putamen, and thalamus (Supplementary Fig. S4). We found that the cortical gradient maps were similar to the original gradient maps, showing a compressed anteriorposterior gradient axis in patients. EOS patients showed decreased covariance between the right putamen (one of the basal ganglia nuclei and part of the striatum) and the 5th bin of the anterior-posterior axis, and increased covariance between the left pallidum and the 3rd bin. However, it is the thalamocortical connectivity that has been shown to strongly contribute to the formation of key characteristics of the mature brain during youth ⁵¹. Our previous work also found increased segregation of macroscale thalamocortical functional organization in EOS⁵². The current coarse resolution of subcortical nuclei may account for the inconsistent findings of the thalamus, and future work examining the cerebellum and finer subcortical regions is highly recommended.

In sum, the current study described a contracted anterior-posterior organization of structural covariance patterns in EOS patients, which may be related to increased distant coordinated changes between posterior regions (including sensorimotor networks) and anterior regions (including transmodal networks such as the DMN and FPN). More broadly, this study suggested a systematic disturbance of maturational processes of cortical thickness in schizophrenia.

Methods

Participants

Ninety-nine drug-naive first-episode EOS patients and 100 TD controls were recruited from the First Hospital of Shanxi Medical University, Taiyuan, China. The diagnosis of schizophrenia was made according to the Structured Clinical Interview for Diagnostic and Statistical Manual of Mental Disorders, Fourth Edition, and confirmed by two senior psychiatrists after at least 6-month follow-up. All patients were at their first episode

period with exhibiting at least one type of positive or negative symptoms for 1–12 months. The psychiatric symptomatology of 71 patients was assessed using the Positive and Negative Syndrome Scale (PANSS). Clinical and imaging data of patients were collected right after baseline diagnosis of schizophrenia to ensure that all data were drug-naive. Next, individualized aggressive medication treatment was implemented under their agreement, in majority of cases with Clozapine, effectively managing symptoms at the lowest possible dose. Both TD controls and their first-degree relatives had no prior history of schizophrenia and were confirmed by the Structured Clinical Interview for DSM-IV Non-Patient Edition. Exclusion criteria for all subjects included (i) age over 18 years; (ii) history of neurological MRI abnormalities; (iii) substance abuse; and (iv) any electronic or metal implants; (v) co-morbid Axis-I or Axis-II disease.

Informed assent was obtained from all pediatric subjects to ensure their knowledge of current condition and treatment, and involving them in appropriate decision-making tasks⁵³. In addition, informed consent was also obtained from their parents or legal guardians⁵⁴. This study was listed on the Chinese Clinical Trial Registry website (registration number: ChiCTR1900025838, https://www.chictr.org.cn/showproj.html?proj=42160) and was approved by the Ethics Committee of the First Hospital of Shanxi Medical University. All ethical regulations relevant to human research participants were followed.

Image data acquisition

T1-weighted anatomical data were collected using a 3 Tesla Siemens MAGNETOM Verio scanner at the First Hospital of Shanxi Medical University. Image data were acquired via a three-dimensional fast spoiled gradient-echo sequence. Scanning parameters included the following: repetition time = 2300 ms, echo time = 2.95 ms, flip angle = 9°, matrix = 256×240 , slice thickness = 1.2 mm (no gap), and voxel size = $0.9375 \times 0.9375 \times 1.2$ mm³, with 160 axial slices.

Cortical thickness extraction

Anatomical images were first preprocessed using the FreeSurfer package (version 7.1.0, http://surfer.nmr.mgh.harvard.edu/)⁵⁵, including cortical segmentation and surface reconstruction. Each anatomical image was visually checked for motion artifacts. Four patients were excluded due to incomplete scanning and one control due to poor quality of cortical parcellation, resulting in a final sample including 95 EOS patients and 99 demographically-matched TD controls (Table 1). Vertex-wise cortical thickness values were then estimated using the distance between the white and pial surfaces. Subsequently, surface vertices were down-sampled to 400 cortical parcels via "Schaefer" local-global atlas⁵⁶. Parcel-wise cortical thickness was estimated by averaging vertex-wise thickness values within each parcel. For each subject, global cortical thickness was calculated by averaging all vertices within the hemispheric mask and was then compared between controls and patients (Supplementary Fig. S3).

Structural covariance gradient calculation

To investigate system-level structural covariance patterns, we computed the structural covariance matrix separately for the EOS and TD groups. Specifically, we computed partial Pearson's correlations between each pair of cross-sectional cortical thickness data with sex, age, and global cortical thickness as covariates. We performed Fisher's z-transformation on the correlation matrix, and then estimated systematic covariance gradients using the BrainSpace toolbox (https://github.com/MICA-MNI/BrainSpace)⁵⁷. Briefly, the z-transformed covariance matrix was column-wise thresholded at 90% and transformed into an affinity matrix by using a normalized angle similarity kernel. Its dimensionality was then nonlinearly reduced by using a diffusion embedding method ($\alpha = 0.5$, a parameter which controls the impact of sampling density)^{26,58}. To make the gradients comparable across individuals, we used a unique gradient mask to align two groups via Procrustes rotations. This mask was generated by the normative TD group for avoiding the influence of disease on gradient directions. The gradient mask based on pediatric subjects was further compared with the well-established

group-level cortical gradient map derived from the HCP adult data, which tends to distinguish posterior cortices from anterior cortices, reflecting the temporal sequence of neurogenesis²⁸. Along the continuous gradient axis, close gradient scores of the two regions reflected similar structural covarying profiles. Additionally, we estimated covariance gradient maps without regressing global cortical thickness (Supplementary Fig. S5), and found similar gradient patterns as the original gradient maps (the first gradient: $r_{(TD)} = 0.95$, $r_{(EOS)} = 0.97$; the second gradient: $r_{(TD)} = 0.81$, $r_{(EOS)} = 0.83$).

Disease effects on structural covariance gradients

To obtain the gradient scores with statistical parameters, we transformed gradient scores to z-scores. We then calculated group-level differences in zscores⁵⁹ and corrected them using the FDR method ($q_{EDR} < 0.05$) to assess statistical significance. The nonparametric Kolmogorov-Smirnov test was used to compare the distributions of gradient scores between the TD and EOS groups⁶⁰. In addition, to characterize the functional involvement of covariance gradients, we further grouped 400 cortical parcels into seven functional networks, including VIS, SMN, dorsal attention network, ventral attention network (VAN), limbic network (LMB), FPN, and DMN⁶¹. Network-level group differences between patients and controls were examined by performing paired t-tests on gradient scores of all parcels belonging to a given network (FDR corrected, $q_{FDR} < 0.05$). To better visualize group differences along the gradient axis, we divided cortical parcels into 10 equal-sized bins according to their ranked gradient scores in TD controls, and performed paired t-tests on gradient scores of all parcels belonging to each bin (FDR corrected, q_{FDR} < 0.05).

Disease effects on structural covariances

To further determine systematic covariance changes in EOS patients, we examined disease effects on structural covariance patterns along the system-level gradient axis. To reduce dimension and aligned to the gradient axis, we first divided cortical parcels into 10 equal-sized bins according to their ranked gradient scores in TD controls. We then averaged the structural covariance matrices within these bins, resulting in 10×10 covariance matrices. Next, we examined diagnosis effects by using a classical linear interaction model with diagnosis and cortical thickness as two factors, as implemented in BrainStat (https://github.com/MICA-MNI/BrainStat) 62 . Finally, we examined symptom effects in the EOS group by using PANSS positive (or negative) scores and cortical thickness as the two factors. In these linear models, sex, age, and global cortical thickness were regressed out, and FDR corrections ($q_{FDR} < 0.05$) were used to control for the effect of false positives.

Relationships with geodesic distances

To evaluate the relationship between systematic structural covariance and physical distance, we first computed the geodesic distance matrix across the cortex. The geodesic distance between two parcels refers to the length of their shortest path on the mesh-based representation of the cortex. Specifically, we computed the geodesic distance between each vertex in fsaverage5 space, and then took the average distance between both parcels to obtain parcel-wise distances by using the Micapipe toolbox (https://micapipe.readthedocs.io/)⁶³. Intra-hemispheric geodesic distances were separately calculated within the left hemisphere and the right hemisphere. Given inter-hemispheric geodesic distance could not be directly measured, they were represented by averaged intra-hemispheric geodesic distances across two hemispheres. We found this averaging step had little influence on following results (Supplementary Fig. S6). We then calculated Pearson's correlations between the gradient maps in TD and the node-wise degree map of geodesic distance. Statistical significance ($p_{spin} < 0.05$) was estimated by using the spin test implemented in the ENIGMA toolbox (https://enigma-toolbox.readthedocs.io/en/latest/)64,65. The spin test simulates 10,000 surrogate surface maps with spatial autocorrelation and generates a null distribution of correlation values. We also computed Pearson's correlation between the structural covariance matrix in TD and the edge-wise geodesic distance matrix, and assessed the significance by using a permutation test ($p_{perm} < 0.05$, 10,000 times).

Table 1 | Demographic and clinical characteristics

Characteristic	TD	EOS	Group comparisons	
			Statistic values	P values
Demographic sample size	99	95	_	-
Handedness (right/ left)	99/0	95/0	_	_
Age range (years)	7–17 years old		-	-
Sex (male/female)	38/61	36/59	0.005 ^a	0.94
Age (years)	14.32 ± 2.08	14.61 ± 1.96	4381 ^b	0.41
Global cortical thickness (mm)	2.62 ± 0.46	2.58 ± 0.45	2.41 °	0.02
Clinical sample size	_	71	_	_
PANSS-T scores	-	65.20 ± 16.92	-	-
PANSS-G scores	_	31.52 ± 8.45	_	_
PANSS-P scores	_	15.37 ± 5.06	_	_
PANSS-N scores	-	13.82 ± 5.51	_	_

Note: Mean + SD.

Disease effects on covariance distances

To further elucidate system-level covariance changes in EOS, we estimated disease effects on covariance distances. Covariance distance refers to the averaged geodesic distance from a seed region to its structurally covarying regions³⁷. Specifically, a column-wise 90%-threshold structural covariance matrix was used as a mask to average the geodesic distance profiles of each parcel to generate the covariance distance map. A high covariance distance score of a seed region reflected a distant projection pattern, while a low score indicated a local projection. Group-level differences between covariance distances of TD and EOS were measured by comparing *z*-score maps of the covariance distance between two groups. In addition, we tested for disease effects by performing paired *t*-tests on covariance distance scores of all parcels belonging to a given gradient bin (q_{FDR} <0.05).

Reporting summary

Further information on research design is available in the Nature Portfolio Reporting Summary linked to this article.

Data availability

Structural covariance patterns and systematic gradient maps in TD and EOS and other data supporting the findings of this study are available at https://github.com/Yun-Shuang/Structural-covariance-gradient-SZ.

Code availability

Custom code was made publicly available under https://github.com/Yun-Shuang/Structural-covariance-gradient-SZ. Gradients calculation is based on BrainSpace (https://brainspace.readthedocs.io/en/latest/). Statistically analyses were performed using BrainStat (https://github.com/MICA-MNI/BrainStat) and ENIGMA. Visualizations were based on the workbench (https://www.humanconnectome.org/software/connectome-workbench) combined with ColorBrewer (https://github.com/scottclowe/cbrewer2).

Received: 14 October 2024; Accepted: 13 May 2025; Published online: 21 May 2025

References

- Stephan, K. E., Friston, K. J. & Frith, C. D. Dysconnection in schizophrenia: from abnormal synaptic plasticity to failures of selfmonitoring. Schizophr. Bull. 35, 509–527 (2009).
- Rapoport, J. L., Giedd, J. N. & Gogtay, N. Neurodevelopmental model of schizophrenia: update 2012. Mol. Psychiatry 17, 1228–1238 (2012).

- Jacobsen, L. K. & Rapoport, J. L. Research update: childhood-onset schizophrenia: implications of clinical and neurobiological research. *J. Child Psychol. Psychiatry* 39, 101–113 (1998).
- Greenstein, D. et al. Childhood onset schizophrenia: cortical brain abnormalities as young adults. *J. Child Psychol. Psychiatry* 47, 1003–1012 (2006).
- Voets, N. L. et al. Evidence for abnormalities of cortical development in adolescent-onset schizophrenia. *NeuroImage* 43, 665–675 (2008).
- Shafiei, G. et al. Spatial patterning of tissue volume loss in schizophrenia reflects brain network architecture. *Biol. Psychiatry* 87, 727–735 (2020).
- Chopra, S. et al. Network-based spreading of gray matter changes across different stages of psychosis. *JAMA Psychiatry* 80, 1246–1257 (2023).
- Georgiadis, F. et al. Connectome architecture shapes large-scale cortical alterations in schizophrenia: a worldwide ENIGMA study. *Mol. Psychiatry*, https://doi.org/10.1038/s41380-024-02442-7 (2024).
- Raznahan, A. et al. Patterns of coordinated anatomical change in human cortical development: a longitudinal neuroimaging study of maturational coupling. *Neuron* 72, 873–884 (2011).
- Schmitt, J. E. et al. Variance decomposition of MRI-based covariance maps using genetically informative samples and structural equation modeling. *NeuroImage* 47, 56–64 (2009).
- Draganski, B. et al. Neuroplasticity: changes in grey matter induced by training. Nature 427, 311–312 (2004).
- Saberi, A. et al. The regional variation of laminar thickness in the human isocortex is related to cortical hierarchy and interregional connectivity. *PLoS Biol.* 21, e3002365 (2023).
- Alexander-Bloch, A., Raznahan, A., Bullmore, E. & Giedd, J. The convergence of maturational change and structural covariance in human cortical networks. *J. Neurosci.* 33, 2889–2899 (2013).
- Khundrakpam, B. S. et al. Exploring individual brain variability during development based on patterns of maturational coupling of cortical thickness: a longitudinal MRI study. Cereb. Cortex 29, 178–188 (2019).
- Khundrakpam, B. S. et al. Imaging structural covariance in the development of intelligence. NeuroImage 144, 227–240 (2017).
- Vijayakumar, N. et al. Cortico-amygdalar maturational coupling is associated with depressive symptom trajectories during adolescence. Neurolmage 156, 403–411 (2017).

TD typically developing controls, EOS early-onset schizophrenia patients, PANSS-T total scores of the positive and negative syndrome scale (PANSS), PANSS-G PANSS general scores, PANSS-P PANSS positive scores, PANSS-N PANSS negative scores.

^aThe χ^2 value for gender distribution was obtained by chi-square test.

The U values were obtained by Mann-Whitney test.

^cThe T values were obtained by two-sample t test.

- Rakesh, D., Elzeiny, R., Vijayakumar, N. & Whittle, S. A longitudinal study of childhood maltreatment, subcortical development, and subcortico-cortical structural maturational coupling from early to late adolescence. *Psychol. Med.* 53, 7525–7536 (2023).
- Prasad, K. et al. Structural covariance networks in schizophrenia: a systematic review Part I. Schizophr. Res. 240, 1–21, https://doi.org/ 10.1016/j.schres.2021.11.035 (2022).
- 19. Prasad, K. et al. Structural covariance networks in schizophrenia: a systematic review Part II. Schizophr. Res. **239**, 176–191 (2022).
- Sandini, C. et al. Development of Structural covariance from childhood to adolescence: a longitudinal study in 22q11.2DS. Front Neurosci. 12, 327 (2018).
- Zalesky, A. et al. Delayed development of brain connectivity in adolescents with schizophrenia and their unaffected siblings. *JAMA Psychiatry* 72, 900–908 (2015).
- Sydnor, V. J. et al. Neurodevelopment of the association cortices: patterns, mechanisms, and implications for psychopathology. *Neuron* 109, 2820–2846 (2021).
- Hilgetag, C. C. & Goulas, A. Hierarchy in the organization of brain networks. *Philos. Trans. R. Soc. Lond. B Biol. Sci.* 375, 20190319 (2020).
- Huntenburg, J. M., Bazin, P. L. & Margulies, D. S. Large-scale gradients in human cortical organization. *Trends Cogn. Sci.* 22, 21–31 (2018).
- Economo, C. F. V. Zellaufbau der Grosshirnrinde des Menschen: Zehn Vorlesungen. (No Title) (1927).
- Margulies, D. S. et al. Situating the default-mode network along a principal gradient of macroscale cortical organization. *Proc. Natl Acad. Sci. USA* 113, 12574–12579 (2016).
- Bernhardt, B. C., Smallwood, J., Keilholz, S. & Margulies, D. S. Gradients in brain organization. *NeuroImage* 251, 118987 (2022).
- Valk, S. L. et al. Shaping brain structure: genetic and phylogenetic axes of macroscale organization of cortical thickness. Sci. Adv. 6, https://doi.org/10.1126/sciadv.abb3417 (2020).
- Kharabian Masouleh, S., Plachti, A., Hoffstaedter, F., Eickhoff, S. & Genon, S. Characterizing the gradients of structural covariance in the human hippocampus. *NeuroImage* 218, 116972 (2020).
- 30. Elston, G. N. Pyramidal cells of the frontal lobe: all the more spinous to think with. *J. Neurosci.* **20**, RC95 (2000).
- Hettwer, M. D. et al. Coordinated cortical thickness alterations across six neurodevelopmental and psychiatric disorders. *Nat. Commun.* 13, 6851 (2022).
- Ercsey-Ravasz, M. et al. A predictive network model of cerebral cortical connectivity based on a distance rule. *Neuron* 80, 184–197 (2013).
- Markov, N. T. et al. Weight consistency specifies regularities of macaque cortical networks. Cereb. Cortex 21, 1254–1272 (2011).
- Barone, P., Batardiere, A., Knoblauch, K. & Kennedy, H. Laminar distribution of neurons in extrastriate areas projecting to visual areas V1 and V4 correlates with the hierarchical rank and indicates the operation of a distance rule. *J. Neurosci.* 20, 3263–3281 (2000).
- 35. Mesulam, M. M. From sensation to cognition. *Brain* **121**, 1013–1052 (1998).
- Barbas, H. General cortical and special prefrontal connections: principles from structure to function. *Annu Rev. Neurosci.* 38, 269–289 (2015).
- Lariviere, S. et al. Functional connectome contractions in temporal lobe epilepsy: Microstructural underpinnings and predictors of surgical outcome. *Epilepsia* 61, 1221–1233 (2020).
- van Haren, N. E. et al. Changes in cortical thickness during the course of illness in schizophrenia. *Arch. Gen. Psychiatry* 68, 871–880 (2011).
- Dong, H. M., Margulies, D. S., Zuo, X. N. & Holmes, A. J. Shifting gradients of macroscale cortical organization mark the transition from childhood to adolescence. *Proc. Natl. Acad. Sci. USA* 118, https://doi. org/10.1073/pnas.2024448118 (2021).

- Dong, D. et al. Compressed sensorimotor-to-transmodal hierarchical organization in schizophrenia. *Psychol. Med.* 53, 771–784 (2023).
- 41. Javitt, D. C. & Freedman, R. Sensory processing dysfunction in the personal experience and neuronal machinery of schizophrenia. *Am. J. Psychiatry* **172**, 17–31 (2015).
- 42. Mesulam, M.-M. E. *Principles of behavioral and cognitive neurology* 2nd edn (Oxford University Press, 2000).
- Marder, E. & Goaillard, J. M. Variability, compensation and homeostasis in neuron and network function. *Nat. Rev. Neurosci.* 7, 563–574 (2006).
- 44. Oligschlager, S. et al. Gradients of connectivity distance are anchored in primary cortex. *Brain Struct. Funct.* **222**, 2173–2182 (2017).
- Wang, Y. et al. Long-range functional connections mirror and link microarchitectural and cognitive hierarchies in the human brain. *Cereb. Cortex* 33, 1782–1798 (2023).
- Oligschlager, S. et al. Gradients of connectivity distance in the cerebral cortex of the macaque monkey. *Brain Struct. Funct.* 224, 925–935 (2019).
- Buckner, R. L. & Krienen, F. M. The evolution of distributed association networks in the human brain. *Trends Cogn. Sci.* 17, 648–665 (2013).
- Jiang, L. et al. Local-to-remote cortical connectivity in early- and adulthood-onset schizophrenia. *Transl. Psychiatry* 5, e566 (2015).
- 49. Sporns, O. Network attributes for segregation and integration in the human brain. *Curr. Opin. Neurobiol.* **23**, 162–171 (2013).
- van Erp, T. G. et al. Subcortical brain volume abnormalities in 2028 individuals with schizophrenia and 2540 healthy controls via the ENIGMA consortium. *Mol. Psychiatry* 21, 585 (2016).
- Park, S. et al. A shifting role of thalamocortical connectivity in the emergence of cortical functional organization. *Nat. Neurosci.* 27, 1609–1619 (2024).
- Fan, Y. S. et al. Macroscale thalamic functional organization disturbances and underlying core cytoarchitecture in early-onset schizophrenia. Schizophr. Bull. 49, 1375–1386 (2023).
- Diekema, D. S., Mercurio, M. R. & Adam, M. B. Clinical Ethics in Pediatrics: A Case-Based Textbook (Cambridge University Press, 2011).
- 54. Cotrim, H., Granja, C., Carvalho, A. S., Cotrim, C. & Martins, R. Children's understanding of informed assents in research studies. *Healthcare* **9**, https://doi.org/10.3390/healthcare9070871 (2021).
- 55. Fischl, B. FreeSurfer. Neurolmage 62, 774-781 (2012).
- Schaefer, A. et al. Local-global parcellation of the human cerebral cortex from intrinsic functional connectivity MRI. Cereb. Cortex 28, 3095–3114 (2018).
- Vos de Wael, R. et al. BrainSpace: a toolbox for the analysis of macroscale gradients in neuroimaging and connectomics datasets. Commun. Biol. 3, 103 (2020).
- Paquola, C. et al. Microstructural and functional gradients are increasingly dissociated in transmodal cortices. *PLoS Biol.* 17, e3000284 (2019).
- Paternoster, R., Brame, R., Mazerolle, P. & Piquero, A. Using the correct statistical test for the equality of regression coefficients. *Criminology* 36, 859–866 (1998).
- Karson, M. Handbook of methods of applied statistics. Volume I: techniques of computation descriptive methods, and statistical inference. Volume II: planning of surveys and experiments. I. M. Chakravarti, R. G. Laha, and J. Roy, New York, John Wiley; 1967, \$9.00. *J. Am. Stat. Assoc.* 63, 1047–1049 (1968).
- Yeo, B. T. et al. The organization of the human cerebral cortex estimated by intrinsic functional connectivity. *J. Neurophysiol.* 106, 1125–1165 (2011).
- Lerch, J. P. et al. Mapping anatomical correlations across cerebral cortex (MACACC) using cortical thickness from MRI. *NeuroImage* 31, 993–1003 (2006).

- Cruces, R. R. et al. Micapipe: A pipeline for multimodal neuroimaging and connectome analysis. *NeuroImage* 263, 119612 (2022).
- 64. Lariviere, S. et al. The ENIGMA toolbox: multiscale neural contextualization of multisite neuroimaging datasets. *Nat. Methods* **18**, 698–700 (2021).
- Alexander-Bloch, A. F. et al. On testing for spatial correspondence between maps of human brain structure and function. *NeuroImage* 178, 540–551 (2018).

Acknowledgements

We are grateful to all the participants and their guardians in this study. We thank International Science Editing (http://www.internationalscienceediting. com) for editing this manuscript. This work was supported by the National Natural Science Foundation of China (62403105, 62333003, 82121003, 62373079), the China Postdoctoral Science Foundation (2023M740524), Sichuan Province Innovative Talent Funding Project for Postdoctoral Fellows, and Medical-Engineering Cooperation Funds from the University of Electronic Science and Technology of China (ZYGX2021YGLH201). S.L.V. was also funded in part by Helmholtz Association's Initiative and Networking Fund under the Helmholtz International Lab grant agreement InterLabs-0015, and the Canada First Research Excellence Fund (CFREF Competition 2, 2015-2016) awarded to the Healthy Brains, Healthy Lives initiative at McGill University, through the Helmholtz International BigBrain Analytics and Learning Laboratory (HIBALL). B.W. was supported by the International Max Planck Research School on Neuroscience of Communication: Function, Structure, and Plasticity (IMPRS NeuroCom).

Author contributions

Yun-Shuang Fan, Sofie Louise Valk, and Huafu Chen contributed to the conception and design of the work. Yong Xu, Mi Yang contributed to the acquisition and interpretation of data for the work. Yun-Shuang Fan, Wei Sheng and Chong Wang contributed to the analysis of data. Yun-Shuang Fan drafted the work. Sofie Louise Valk, Bin Wan, and Huafu Chen revised it critically for important intellectual content.

Competing interests

The authors declare no competing interests.

Additional information

Supplementary information The online version contains supplementary material available at https://doi.org/10.1038/s42003-025-08216-3.

Correspondence and requests for materials should be addressed to Sofie Louise Valk or Huafu Chen.

Peer review information Communications Biology thanks Sunaina Soni and the other anonymous reviewer(s) for their contribution to the peer review of this work. Primary Handling Editors: Christina Karlsson Rosenthal. A peer review file is available.

Reprints and permissions information is available at http://www.nature.com/reprints

Publisher's note Springer Nature remains neutral with regard to jurisdictional claims in published maps and institutional affiliations.

Open Access This article is licensed under a Creative Commons Attribution-NonCommercial-NoDerivatives 4.0 International License, which permits any non-commercial use, sharing, distribution and reproduction in any medium or format, as long as you give appropriate credit to the original author(s) and the source, provide a link to the Creative Commons licence, and indicate if you modified the licensed material. You do not have permission under this licence to share adapted material derived from this article or parts of it. The images or other third party material in this article are included in the article's Creative Commons licence, unless indicated otherwise in a credit line to the material. If material is not included in the article's Creative Commons licence and your intended use is not permitted by statutory regulation or exceeds the permitted use, you will need to obtain permission directly from the copyright holder. To view a copy of this licence, visit http://creativecommons.org/licenses/by-nc-nd/4.0/.

© The Author(s) 2025